Mechatronics 88 (2022) 102897

Contents lists available at ScienceDirect

Mechatronics

journal homepage: www.elsevier.com/locate/mechatronics

Coupled stability analysis of cascaded leader–follower teleoperation networks using Möbius transformation ☆

Kamran Razi [a], Chiedu N. Mokogwu [b,*], Keyvan Hashtrudi-Zaad [b]

[a] Fortinet Inc., Burnaby, Canada
[b] Department of Electrical and Computer Engineering, Queen's University, Kingston, ON K7L 3N6, Canada

ARTICLE INFO

Keywords:
Teleoperation
Cascaded networks
Absolute stability
Möbius transformation
Passivity
Time delay

ABSTRACT

In this paper, we use the notion of Möbius transformation to develop a chain-wise methodology for the analysis of coupled stability in a cascade of leader–follower networks. The methodology tracks the transmission of the load passivity unit disk through the cascade to the user network. It allows for networks in the cascade that are neither passive nor absolutely stable. Due to its modularity, the proposed methodology is more suitable for dynamic distributed systems in which a network block, such as virtual coupling or delay in the cascade, is modified, added or taken out. We also introduce the notion of *"bounded-Γ absolute stability"* to verify the coupled stability for any prescribed range of loads, denoted by circles in the scattering domain. To demonstrate the effectiveness of the proposed methodologies, numerical and experimental results for a position–force control architecture under constant time delays are provided.

1. Introduction

Teleoperation has found applications in various areas including remote space operations, [1], exploring deep sea, [2], handling nuclear materials, [3], motion/power scaling for cell manipulation [4,5], robotic tele-rehabilitation for post-stroke survivors [6], added maneuverability in minimally invasive surgery [7], and MRI-compatible leader–follower systems for surgical procedures [8].

The stability of teleoperation systems is often analyzed using the network model of these systems, which includes a two-port leader–follower network (LFN) interacting with the operator and environment one-port networks, as seen in Fig. 1. The stability of LFN coupled to often varying and unknown dynamics of the environment and the operator is challenging and of paramount importance.

The uncertain dynamics of environments are often dealt with under the passivity umbrella. Human operator arm often exhibits complex, time-varying and nonlinear behavior. However, it has been argued that human operator arm maintains stable touch with passive objects [9]. As a result, the coupled system will be stable as long as the dynamics experienced by the operator for all passive environment loads is passive. Since interconnection of passive networks is stable [6,10], one solution is to design for a passive LFN [11]. This solution is conservative as it ensures that maximum energy extractable from network ports are limited. A less conservative set of necessary and sufficient conditions for two-port LFNs can be derived from utilizing absolute stability. Absolute stability guarantees coupled stability for any given passive environment. The most widely employed absolute stability method is the Llewellyn's Absolute Stability (A.S) criterion [12,13]. A sizable body of past research considers A.S. analysis of lumped two-port LFNs [14–17] and more recently extensions to multi-port LFNs using Llewellyn's criterion [18,19], Integral Quadratic Constraints (IQC) formulation [20], Zeheb–Walach criteria [21], and absolute k-stability [22]. Recently a data-driven method for experimental evaluation of absolute stability in telerobotic systems has been proposed [23]. In this method, an alternative approach to assess absolute stability is accomplished by conducting at most three sets of experiments with the follower in free motion, mass-carrying, and locked, as in interacting with a rigid environment.

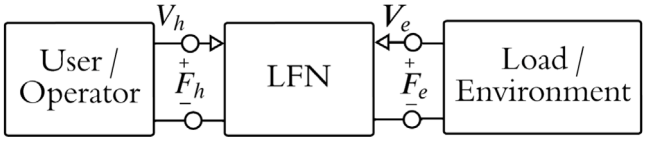

Fig. 1. Network representation of a teleoperation system showing the human operator (user) in contact with a LFN in contact with a load (environment).

☆ This paper was recommended for publication by Associate Editor Jee-Hwan Ryu.

* Corresponding author.
E-mail addresses: razi.kamran@gmail.com (K. Razi), chiedu.mokogwu@queensu.ca (C.N. Mokogwu), khz@queensu.ca (K. Hashtrudi-Zaad).

https://doi.org/10.1016/j.mechatronics.2022.102897
Received 8 October 2021; Received in revised form 21 August 2022; Accepted 12 September 2022
Available online 3 October 2022

As the teleoperation technology progresses and its applications grow, the network representation of these systems becomes more involved. For example, a traditional leader–follower system may have multiple two-port networks in between the leader and follower to represent the system hardware (e.g. tools), or to meet certain kinesthetic performance requirements (e.g. virtual couplings or intermittent impedances) or stability requirements (e.g. wave variable transformations) [14,24–26]. As another example, consider a multiple-leader, multiple-follower configuration where two operators manipulate a task through their leader–follower teleoperation systems [27,28]. The network representation of such a system involves a cascade of two two-port networks associated with two leaders, two followers and an environment connecting two one-port operator networks [29].

Applying Llewellyn's criterion involves obtaining the two-port network representation of the entire cascade between the operator and the environment, or between the two operators, respectively. In addition, if one of the two-port networks go under any change, the entire stability analysis needs to be redone.

The coupled stability of the cascade of subnetworks can be achieved by guaranteeing the passivity or absolute stability of each subnetworks. Agrawal et al. proposed the verification of compositional passivity for cascaded interconnected nonlinear systems [30]. Razi and Hashtrudi-Zaad proposed a framework to synthesize a guaranteed stable multi-leader multi-follower teleoperation system from the interconnection of absolutely stable leader and follower subnetworks [22]. A similar process has been adopted for vehicle platoons, which are composed of a cascade of the dynamics and controllers for each vehicle [31]. In such systems, the output strict passivity (OSP) of each vehicle subsystem being upper-bounded by unity leads to guaranteed vehicle L_2-stability and as a result strong string stability. Although in these approaches the passivity or absolute stability of each subnetwork is considered independently of other subnetworks, it will result in conservative teleoperation coupled stability conditions. Alternatively, the above-mentioned A.S. methods, such as the Llewellyn's criterion, can be applied to the two-port network representation of the entire cascade between the operator and the environment, or between the two operators, respectively. However, if one of the two-port networks go under any change, the entire stability analysis needs to be redone.

This work proposes an alternative modular approach to ensure the A.S of the entire LFN, while addressing the above issues. A preliminary version of this work was presented at [32]. The proposed methodology considers the cascade of networks $N_1, \dots, N_r$, as shown in Fig. 2, and uses the properties of Möbius transformation to find out how a load, denoted by the reflection coefficient Γ_2, is transmitted to input port (port 1). Starting from the last network in the cascade where the load is denoted by passivity unit circles in the scattering domain, it continues tracking the loci of the circles until it finds the location of the mapped circles at the operator side, that is $\Gamma_{in}^{N_1}$. If these circles are contained in the unit circle, then the network N is A.S; otherwise, it is potentially unstable. In this process, the notion of "bounded-Γ A.S" is introduced which ensures the passivity of the transmitted impedance for a prescribed range of load impedance for the last network.

The proposed methodology has a number of advantages and benefits compared to the other existing methods:

1. It is modular and easy to use, as the Möbius transformation for each subnetwork is relatively simple and only depends on the parameters of that subnetwork, rather than the entire network. Therefore, if a two-port subnetwork is replaced or modified, only the Möbius transformation of that subnetwork needs to be updated, and tracking the circles are only needed for the following subnetworks, rather than redoing the tracking for the entire analysis.
2. This approach applies to cascades of active subnetworks with arbitrary energy mappings, where the traditional absolute stability analyses fail to apply.
3. The proposed method provides a means for graphical verification of absolute stability, which tracks the absolute stability or potential instability of the cascaded network.

The proposed strategy will be investigated through numerical analysis and experiments.

The remainder of this paper proceeds as follows; the definition of Möbius transformation, Symmetry principle and mathematical derivations for helper propositions and corollaries are presented in Section 2. Section 3 introduces absolute stability, its definitions and the main contribution of this paper. A case study utilizing a position–force control architecture, and absolute stability analysis with inclusion of a two-port virtual coupling and time delay is found in Section 4. The experimental setup, results and discussions are found in Section 5, while the conclusions and future work are presented in Section 6.

2. Möbius transformation and coupled stability of a two-port network

In this section, we first present the Möbius transformation and its symmetry principle and show how the principle can be used to find the mapping of a unit circle under this transformation. Then by showing that the input reflection coefficient of a two-port network is a special case of Möbius transformation, the A.S condition of the network in terms of the scattering parameters is derived. Furthermore, the notion of bounded-Γ A.S for the network is introduced which allows for a less conservative design of the network by considering a bounded region of load uncertainty. This notion provides flexibility in the design of a cascade of networks for A.S, where it verifies the A.S of a network for a prescribed region of load rather than the unit passivity disk.

Notation: Throughout this paper we denote time-domain signals by small letters and Laplace-domain signals by capital letters. Furthermore, $f = x \circ y$ refers to the product of a mapping between x and y, C refers to complex number and $C_\infty = C \cup \infty$ and $(.)^*$ refers to the complex conjugate value of its argument.

2.1. Möbius transformation and the symmetry principle

The properties of Möbius transformation have been used in the literature to obtain A.S conditions [23] for networks. Here, we propose a novel alternate method which uses the symmetry principle to obtain a result that will be employed in Section 3.1 to obtain the A.S condition for LFNs. The following definitions, theorems and corollaries lay a foundation upon which we will build our proposed methodology.

Definition 1 (*Möbius Transformation*)**.** Möbius transformation $f : \mathbb{C}_\infty \to \mathbb{C}_\infty$ is a mapping defined as

$$f(z) = \frac{az + b}{cz + d}, \quad a, b, c, d \in \mathbb{C} \tag{1}$$

with the condition $ad - bc \neq 0$.

Definition 2 (*Symmetric Points [33]*)**.** The symmetry of the point $z \notin C(a, r)$ with respect to the circle $C(a, r)$, that is $z^s_{C(a,r)}$, is given by

$$z^s_{C(a,r)} = \begin{cases} \frac{r^2}{z^* - a^*} + a & \text{if} \quad z \neq a \\ \infty & \text{if} \quad z = a, \end{cases} \tag{2}$$

where a and r are the circle center and radius.

Lemma 1 (*Symmetry Principle*)**.** *Given a circle C and the Möbius transformation $f(z)$, the points z_1 and z_2 are symmetric with respect to the circle C if and only if (iff) their images $f(z_1)$ and $f(z_2)$ are symmetric with respect to the image $f(C)$ of C.*

Proof. See [33]. □

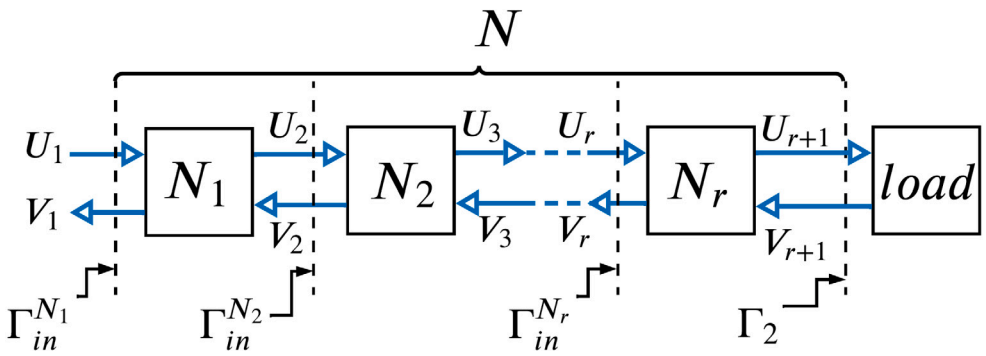

Fig. 2. A.S. analysis of network N through deriving input reflection coefficient of network N_r, that is $\Gamma_{in}^{N_r}$, and tracking it back to the network N_2. Finally, bounded-Γ A.S. of network N_1 concludes A.S. of the entire network N.

The Möbius transformation in (1) can be alternatively shown by

$$f(z) = \frac{a}{c} + \frac{(bc-ad)/c^2}{z+d/c} = \beta + \frac{\rho e^{i\theta}}{z+\alpha}, \tag{3}$$

which states that f is obtained via a composition of translation ($\alpha \in \mathbb{C}$), inversion, dilation ($\rho \in \mathbb{R}$), rotation ($\theta \in \mathbb{R}$), and another translation ($\beta \in \mathbb{C}$). In the following, we derive the image of the circle $C(a_0, r_0)$ under the mapping $f(z)$. We first start with the special case $f_1(z) = 1/(z+\alpha)$. The image is a circle provided that the circle $C(a_0, r_0)$ does not include the pole $-\alpha$ of the transformation, that is $|\alpha - a_0| \neq r_0$. The following proposition summarizes the results.

Proposition 1 (*Circle-to-Circle*). *The Möbius transformation* $f_1(z) = 1/(z+\alpha)$ *maps the circle* $C(a_0, r_0)$ *to the circle* $C(a_1, r_1)$ *with*

$$a_1 = \frac{\alpha^* + a_0^*}{|\alpha + a_0|^2 - r_0^2}, \quad r_1^2 = \frac{r_0^2}{(|\alpha + a_0|^2 - r_0^2)^2} \tag{4}$$

Proof. First we show that mapping of a circle is a circle. It is known that four points are cocyclic iff their cross-ratio is real [34]. Since the Möbius transformation preserves cross-ratio, the mapping of the four points are on a circle as well. From the definition of symmetric points in (2), one can see that the center of the circle a_1 is symmetric to ∞, that is

$$(\infty)^s_{C(a_1,r_1)} = a_1 \tag{5}$$

According to Lemma 1, Möbius transformation preserves the symmetry property. Therefore, the inverse points are symmetric with respect to the circle $C(a_0, r_0)$, and (5) yields

$$(f_1^{-1}(\infty))^s_{C(a_0,r_0)} = f_1^{-1}(a_1) \tag{6}$$

Replacing for

$$(f_1^{-1}(\infty))^s_{C(a_0,r_0)} = (-\alpha)^s_{C(a_0,r_0)} \tag{7}$$

into (2), yields

$$(f_1^{-1}(\infty))^s_{C(a_0,r_0)} = \frac{r_0^2}{-\alpha^* - a_0^*} + a_0 \tag{8}$$

which is equal to the right-hand-side of (6) or

$$a_1 = f_1\left(\frac{r_0^2}{-\alpha^* - a_0^*} + a_0\right) = \frac{\alpha^* + a_0^*}{|\alpha + a_0|^2 - r_0^2}. \tag{9}$$

To obtain the radius r_1, note that ∞ and a_0 are symmetric with respect to $C(a_0, r_0)$. Thus, using Lemma 1, the images under f_1 are symmetric with respect to the image of the circle $C(a_0, r_0)$ which is $C(a_1, r_1)$. In other words,

$$(f_1(\infty))^s_{C(a_1,r_1)} = f_1(a_0) \tag{10}$$

Equating $(f_1(\infty))^s_{C(a_0,r_0)} = (0)^s_{C(a_0,r_0)} = r_1^2/(-a_1^*) + a_1$ to $f_1(a_0) = 1/(a_0+\alpha)$ in (10) and simplifying further gives r_1 in (4). □

The results can now be extended for the mapping $f(z)$ in (3) by considering $f = g \circ (f_1)(z) = g(f_1(z))$ and $g(z) := \rho e^{i\theta} z + \beta$, which is the composition of the similarity transformation g and f_1.

Corollary 1. *The image of the circle* $C(a_0, r_0)$ *under the general Möbius transformation* f *in* (3) *is the circle* $C(a, r)$ *with*

$$a = \rho e^{i\theta} a_1 + \beta, \quad r = |\rho| r_1 \tag{11}$$

where a_1 *and* r_1 *are found from* (4).

Furthermore, the mapping of the interior of the unit circle $C(0, 1)$ can be obtained by considering that $f(-\alpha) = \infty$. Thus, the condition $|\alpha| > 1$ ensures that the exterior of the unit disk maps to the exterior of the circle $C(a, r)$. The result is summarized in the following Corollary.

Corollary 2. *The condition*

$$|\alpha| > 1, \tag{12}$$

ensures that the image of a unit disk maps to the interior of the circle $C(a, r)$. *Adding the condition*

$$|\rho e^{i\theta} a_1 + \beta| + |\rho| r_1 \leq 1, \tag{13}$$

ensures that the image remains within the unit disk. For other properties of Möbius transformation, the reader is referred to [23,33].

In this section, the theoretical foundations have been laid for the proposed method which will be presented in the subsequent sections.

3. Absolute stability

Consider the two-port network N terminated by a load, as shown in Fig. 3, where E_1, E_2, F_1 and F_2 are the cross (effort) and through (flow) variables for port 1 and 2. Absolute stability of a two-port network can be defined as

Definition 3 (*Absolute Stability [35,36]*). A two-port network (LFN) is absolutely stable if there exists no set of passive terminating one-port networks (load) for which the system is unstable.

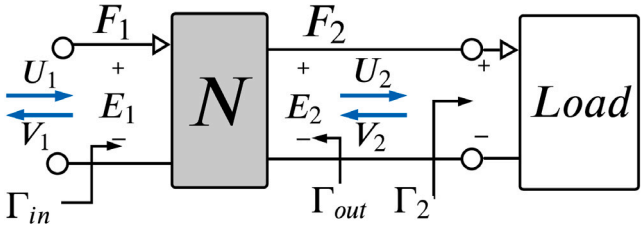

Fig. 3. Network N terminated by a passive load and represented in the scattering domain.

The network N is absolutely stable iff the dynamics viewed from port 1 is passive for all passive loads. If the network is not A.S., it is potentially unstable.

In terms of the network immittance parameters, A.S. can be determined by the Llewellyn's Absolute Stability Criterion:

Theorem 1 (*Llewellyn's Absolute Stability Criterion [13,36]*)**.** *A two-port network represented by the immittance matrix $P = [p_{i,j}]$, $(i, j) = (1, 2)$ is absolutely stable if and only if*

1. *p_{11} and p_{22} have no poles in the right-half plane;*
2. *Any poles of p_{11} and p_{22} on the imaginary axis are simple with real and positive residues;*
3. *For all real values of frequencies ω, $\Re(p_{11}) \geq 0$, $\Re(p_{22}) \geq 0$ and*

$$\eta(\omega) := \frac{2\Re(p_{11})\,\Re(p_{22})}{|p_{12}p_{21}|} - \frac{\Re(p_{12}p_{21})}{|p_{12}p_{21}|} \geq 1 \tag{14}$$

where $|\cdot|$ and $\Re(\cdot)$ denote the absolute and real values of their corresponding arguments and η is the network stability parameter.

In the next section, we apply the results obtained in the previous section to find the A.S. condition of a two-port network in the scattering domain. The results will then be extended to study the A.S. of a chain of cascaded networks in Section 4.

3.1. Absolute stability in scattering domain

Scattering theory is a powerful tool for the analysis of stability of coupled systems. The scattering representation of the network N is defined by

$$\begin{bmatrix} V_1 \\ U_2 \end{bmatrix} = \mathbf{S} \begin{bmatrix} U_1 \\ V_2 \end{bmatrix}, \quad \mathbf{S} = \begin{bmatrix} S_{11} & S_{12} \\ S_{21} & S_{22} \end{bmatrix} \tag{15}$$

where $\mathbf{S}$ is the scattering operator relating the Laplace transform of the incident (U), and reflected (V) waves. The *inwave* or incident wave, $U = [U_1, U_2]$, and the *outwave* or reflected wave $V = [V_1, V_2]$ as shown in Fig. 3 are defined as

$$\begin{cases} U_1 = E_1 + bF_1 \\ U_2 = E_2 + bF_2 \end{cases} \text{ and } \begin{cases} V_1 = E_1 - bF_1 \\ V_2 = E_2 - bF_2 \end{cases}, \tag{16}$$

where $b > 0$ is the characteristic wave impedance.

The reflection coefficient at port 2 or the load reflection coefficient in Fig. 3 is also defined as $\Gamma_2 := \frac{V_2}{U_2}$. The two-dimensional complex plane spun by the reflection coefficient for all possible loads is called the Γ_2-plane. This definition can be expanded to any reflection coefficient. The input reflection coefficient Γ_{in}, i.e. the reflection coefficient at port 2 reflected to port 1, is defined by and derived as [23,37]

$$\Gamma_{in} := \left.\frac{V_1}{U_1}\right|_{V_2=\Gamma_2 U_2} = S_{11} + \frac{S_{12}S_{21}\Gamma_2}{1 - S_{22}\Gamma_2} \tag{17}$$

$$= \frac{-S_{12}S_{21}/S_{22}^2}{\Gamma_2 - 1/S_{22}} + \frac{\Delta}{S_{22}} \tag{18}$$

where $\Delta := S_{11}S_{22} - S_{12}S_{21}$.

The system is absolutely stable iff the dynamics viewed from port 1 is passive, *i.e.* $|\Gamma_{in}| \leq 1$ for all passive loads with Γ_2 that covers the entire unit disk in the Γ_2-plane. The input reflection coefficient $\Gamma_{in}(\Gamma_2)$ in (18) is a mapping in the composition form of Möbius transformation in (3). Replacing for $\alpha = -1/S_{22}$ in the passivity condition set (12) yields

$$|S_{22}| < 1. \tag{19}$$

In addition, replacing for $\beta = \Delta/S_{22}$, and $\rho e^{i\theta} = -S_{12}S_{21}/S_{22}^2$ in (13) yields

$$\left|\frac{-S_{12}S_{21}}{S_{22}^2}\frac{-1/S_{22}^*}{|1/S_{22}|^2 - 1} + \frac{\Delta}{S_{22}}\right| + \frac{|S_{12}S_{21}|}{|S_{22}|^2\left(|1/S_{22}|^2 - 1\right)} < 1 \tag{20}$$

Simplifying (19)–(20) further yields to the following A.S. condition

$$\frac{1 - |S_{22}|^2}{|S_{11} - \Delta S_{22}^*| + |S_{12}S_{21}|} \geq 1 \tag{21}$$

which was first reported in [37].

In the following section, a more flexible and broader definition of A.S. is introduced that considers a bounded set of load impedances rather than the specific load unit disk.

3.2. Bounded-Γ absolute stability

Consider the load Γ_2, with the range denoted by $\bar{\Gamma}_2$ characterized by circles $C(a_{lr}, r_{lr})$ as follows

$$\bar{\Gamma}_2 = \{\Gamma_2 : |\Gamma_2 - a_{lr}| \leq r_{lr}\}. \tag{22}$$

The above definition states that the load Γ_2 is restricted by a disk with the center a_{lr} and radius r_{lr}.

Definition 4 (*Bounded-Γ A.S.*)**.** A network N terminated at port 2 by the load Γ_2 is called bounded-Γ absolutely stable with regards to region $\bar{\Gamma}_2$ iff the input reflection coefficient is limited to the unit disk, i.e. $|\Gamma_{in}| < 1$ for all $\Gamma_2 \in \bar{\Gamma}_2$.

This definition provides a broader coverage for the load than what is stipulated in the definition of A.S. in Definition 3. If the load is the entire passive unit disk, i.e. $|\bar{\Gamma}_2| < 1$, then it matches the definition of A.S. However, $\bar{\Gamma}_2$ in a general case is a bounded set of impedances which can also include active loads. The Bounded-Γ A.S. can also be used for networks that are potentially unstable, where the entire passivity unit disk load does not map to the passive Γ_{in}. In that situation, Bounded-Γ A.S. specifies part of passivity disk in the Γ_2-plane that results in the passive Γ_{in}.

We are interested in a set of conditions on the scattering parameters that ensures $|\Gamma_{in}| < 1$, for a given load region denoted by circles $c(a_{lr}, r_{lr})$. Note that points on the boundary of load region or load circle can be written by

$$\Gamma_{2c} := a_{lr} + r_{lr}\Gamma_{uc} \tag{23}$$

where Γ_{uc} denotes points on the unit circle $C(0, 1)$. By replacing for $\Gamma_2 = \Gamma_{2c}$ in (18), the mapping $\Gamma_{inc} = \Gamma_{in}(\Gamma_{2c})$ can be written by

$$\Gamma_{inc} = \frac{-S_{12}S_{21}/(S_{22}^2 r_{lr})}{\Gamma_{uc} + \frac{a_{lr}}{r_{lr}} - \frac{1}{S_{22}r_{lr}}} + \frac{\Delta}{S_{22}} \tag{24}$$

which shows the mapping of a circle Γ_{2c} under the Möbius transformation Γ_{inc}. Hence, the centers and the radii of Γ_{inc} can be calculated at each frequency using (4) and (11), where here $a_0 = 0$ and $r_0 = 1$.

Bounded-Γ A.S. can be checked using the notion of Γ_2-stability region $\bar{\Gamma}_{sr}$, which is the set of *all* Γ_2 that maps to a passive Γ_{in} [15] or

$$\bar{\Gamma}_{sr} = \{\Gamma_2 : |\Gamma_{in}| \leq 1\}, \tag{25}$$

see Fig. 4. In effect, $\bar{\Gamma}_{sr}$ represents all linear dynamic terminations, whether passive and/or active, that are experienced at the input port of the network N as passive dynamics or impedances. This will guarantee the stability of the network N coupled from the left to any passive network. To obtain the stability region $\bar{\Gamma}_{sr}$, we first solve (18) for Γ_2 to obtain

$$\Gamma_2 = \frac{-S_{12}S_{21}/S_{22}^2}{\Gamma_{in} - \Delta/S_{22}} + \frac{1}{S_{22}} \tag{26}$$

Now, denote the Möbius transformation mapping $\Gamma_{src} = C(a_{sr}, r_{sr})$ for the boundary $\Gamma_{in} = \Gamma_{uc}$ from (25). $\bar{\Gamma}_{src}$ represents all linear dynamic terminations Γ_2 that map to unit passivity circle at the input port. From Corollary 2, to the interior of Γ_{in} maps to interior or exterior of Γ_{src}

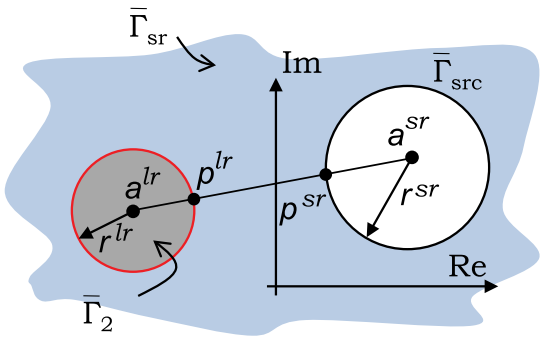

Fig. 4. Verification of bounded-Γ A.S. by checking if the Γ_2 load range ($\bar{\Gamma}_2$) is included within the stability region representing all dynamic terminations $\bar{\Gamma}_{sr}$. This is shown by the shaded area outside of circle $C(a_{lr}, r_{lr})$ ($|\beta| < 1$). Network N is bounded-Γ A.S. iff $|a_{lr} - a_{sr}| \geq r_{sr} + r_{lr}$ for $|\beta| < 1$ and if $|a_{lr} - a_{sr}| \leq r_{sr} - r_{lr}$ for $|\beta| > 1$. The relative distance $|p_{lr} - p_{sr}|$ is a measure of robustness to load variations.

for $\Delta/S_{22} < 1$ or $\Delta/S_{22} > 1$, respectively. These two cases can be summarized by the following equation

$$\bar{\Gamma}_{sr} : (|\Gamma_2 - a_{sr}| - r_{sr})(1 - |\beta|) > 0 \tag{27}$$

where $\beta = \Delta/S_{22}$ is the pole of the transformation.

In Bounded-Γ A.S., the region of interest in the Γ-plane, that is $\bar{\Gamma}_2$, is a specific region and a subset of all Γ_2's that maps to a passive Γ_{in}. Therefore, verifying bounded-Γ A.S. checks for the inclusion of the load range $\bar{\Gamma}_2$ in $\bar{\Gamma}_{sr}$. The above discussion leads to the following proposition.

Proposition 2. *Given network N terminated at port 2 by the reflection coefficient $\bar{\Gamma}_2 \in \Gamma_2$, defined in (22), the network N is said to be bounded-Γ A.S. with regards to the load region $\bar{\Gamma}_2$ iff*

$$\begin{aligned} &|a_{lr} - a_{sr}| \geq r_{sr} + r_{lr} \quad \textit{for} \quad |\beta| < 1 \\ &|a_{lr} - a_{sr}| \leq r_{sr} - r_{lr} \quad \textit{for} \quad |\beta| > 1. \end{aligned} \tag{28}$$

Proof of Sufficiency. Fig. 4 illustrates the relative representation of $\bar{\Gamma}_{sr}$ and $\bar{\Gamma}_2$ for ($|\beta| < 1$). For bounded-Γ A.S., $\bar{\Gamma}_{2c}$ must stay fully outside Γ_{src}, and from (27), this requires that $|\Gamma_{2c} - a_{sr}| > r_{sr}$. In other words, the distance from any point on Γ_{2c} to a_{sr} be larger than r_{sr}. For all the points on Γ_{2c}, the minimum of $|\bar{\Gamma}_{2c} - a_{sr}|$ is $|a_{lr} - a_{sr}| - r_{lr}$. This implies that if $|a_{lr} - a_{sr}| > r_{sr} + r_{lr}$, that the condition (27) is satisfied for $|\beta| > 1$, $\bar{\Gamma}_{2c}$ must stay fully within Γ_{src}. From (27), this requires that $|\Gamma_{2c} - a_{sr}| < r_{sr}$. For all the points on Γ_{2c}, the maximum of $|\Gamma_{2c} - a_{sr}|$ is $|a_{lr} - a_{sr}| + r_{lr}$. This implies that if $|a_{lr} - a_{sr}| < r_{sr} + r_{lr}$, then the condition (27) is satisfied. □

Proof of Necessity. Γ_{sr} includes all load regions for which reflection coefficient Γ_{in} renders passive. For the case of $|\beta| < 1$ as presented in Fig. 4, if the load boundary Γ_{2c} denoted by the circle $C(a_{lr}, r_{lr})$ does not satisfy (1), it intersects with the circle $C(a_{sr}, r_{sr})$. That is the load Γ_2 is not in the stability region given by the region in the exterior of the circle $C(a_{sr}, r_{sr})$. Necessity proof for (2) is similar. □

For the non-intersecting circles in Fig. 4, the points p_{lr} and p_{sr} are the intersection of the circles $C(a_{lr}, r_{lr})$ and $C(a_{sr}, r_{sr})$ with the line connecting the centers. For a given network N, the distance between p_{lr} and p_{sr} over the frequency range denotes the robustness to the load variations. This is because the load circle Γ_{2c} and the stability circle Γ_{src} must be non-overlapping; in other words, as the load changes and the size and location of Γ_{2c} varies, the distance $|p_{lr} - p_{sr}|$ should not shrink to zero. Therefore, the larger $|p_{lr} - p_{sr}|$, the larger will be the robustness of bounded-Γ absolute stability of the network to load variations.

3.3. Absolute stability of interconnected networks

Consider the network N in Fig. 2, which is composed of r cascaded networks N_1 through N_r. The cascade representation of the network N is inspired by the underlying physical components of the system that are connected at their ports and exchange energy. It often happens that a block is introduced within the cascade. Examples include the existence of time delay between the leader and follower or the addition of virtual coupling for enhanced performance [14], these two examples will be applied to the case study that we investigate in Section 4. The A.S. analysis of the network can be done by applying the exiting techniques such as Llewellyn's to the immittance model of the lumped network N. Also, any changes in the network including adding or removing components requires deriving the modified N and repeating the entire stability analysis.

An alternate method that enables a modular analysis of A.S. of the system is to ensure the A.S. of each of the networks N_1 to N_r. Network N_r is terminated by any passive load Γ_2. The A.S. of N_r ensures the passivity of the input reflection coefficient $\Gamma_{in}^{N_r}$. Following this line of thought and considering the A.S. of each of networks N_{r-1} through N_1 ensures the passivity of $\Gamma_{in}^{N_1}$, as a result the A.S. of N. This approach is conservative in the sense that not all the subnetworks need to be A.S. for the cascade N to be A.S.

To obtain a less conservative modular stability analysis of the cascaded networks, we propose a chain-wise method that uses the Möbius transformation property of the mapping that transforms the load side of each subnetwork to its input side. We first start from network N terminated by load Γ_2. For all passive loads Γ_2, Eq. (18) gives the range of coefficient $\Gamma_{in}^{N_r}$, denoted by circles $C(a_{N_r}, r_{N_r})$. These circles characterize the range of the load for the next network in the chain, that is N_{r-1}. We continue this process by tracking these circles through the networks $N_r, \ldots, N_2$ to obtain the range of load for N_1, denoted by $C(a_{N_1}, r_{N_1})$. Now, bounded-Γ A.S. of N_1 with regards to circles $C(a_{N_1}, r_{N_1})$ ensures that $|\Gamma_{in}^{N_1}| < 1$. In other words,

$$\Gamma_{in}^{N_2} \in \bar{\Gamma}_{sr}^{N_1} \quad \text{for all } |\Gamma_2| < 1 \tag{29}$$

which ensures A.S. of the lumped network N.

This proposed method is less conservative compared to ensuring the A.S. of each of the networks N_1 to N_r, as it aims at A.S. of the entire network, rather than the subnetworks. It also benefits from simpler analysis by looking at smaller simpler subnetworks composing the lumped network N. Each subnetwork N_i includes one or a set of control parameters that alter the mapping of $\Gamma_{in}^{N_i}$, denoted by circles $C(a_{N_i}, r_{N_i})$. Studying the effect of each parameter on altering the corresponding mapping can be conducted for each subnetwork individually. This benefit facilitates the design of controllers for stability, which will be shown through an example for delayed systems in Section 4.3.

Other advantages of the proposed method are that the mapping $\Gamma_{in}^{N_i}$ can be used

(i) to track the absolute stability or potential instability of the cascade of networks $N_r, \ldots, N_i$, and
(ii) to qualitatively argue about the effective amount of dissipative components in the cascade network $N_r, \ldots, N_i, i = 1, \ldots, r$.

The reason for the latter is that for each frequency the size and the location of the circles of $\Gamma_{in}^{N_i}$ is determined by the real part or resistive part of $\Gamma_{in}^{N_i}$, which is indicative of the dissipation in the cascade $N_r, \ldots, N_i$ [15]. As the effective damping increases, the circles become smaller and closer to the point $(1, j0)$. Therefore if we observe the size of the circles shrinks and their locations become closer to $(1, j0)$ as we proceed with our mappings towards N_1, then one can qualitatively conclude that the system is adding more dissipating elements from right to left to guarantee the A.S. of the entire network.

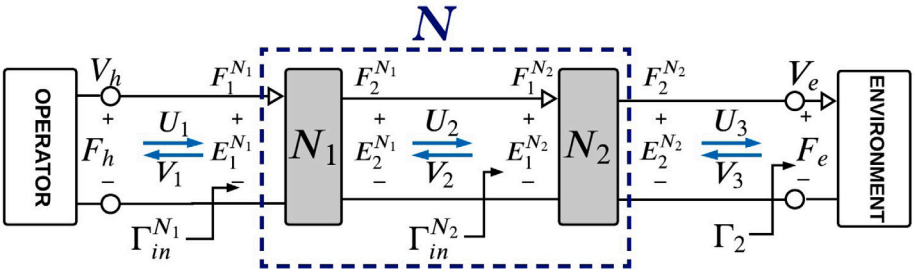

Fig. 5. Distributed representation of network N for the P-F architecture, terminated by passive environment load and the operator.

4. Case study

The proposed chain stability analysis is examined on a classic P-F control architecture. The benefit of the proposed coupled stability method in handling changes to the cascade is demonstrated by adding a virtual tool and a delay block between the leader and follower. The delayed system is implemented directly in the power domain, allowing for explicit transmission of position feedback.

4.1. Position–force control architecture

Consider a single degree-of-freedom leader–follower teleoperation system represented by an operator in contact with a leader, a follower interacting with an environment (load), and communications channel through signals are exchanged as seen in Fig. 5. The dynamics of the leader, follower and communications channel are modeled as a two-port network N, which can be represented by the class of immittance matrices, which includes Impedance, $Z(s)$ and Hybrid $H(s)$, defined as follows

$$\begin{bmatrix} F_h \\ F_e \end{bmatrix} = \mathbf{Z}(s) \begin{bmatrix} V_h \\ -V_e \end{bmatrix}, \mathbf{Z}(s) = \begin{bmatrix} z_{11} & z_{12} \\ z_{21} & z_{22} \end{bmatrix},$$
$$\begin{bmatrix} F_h \\ -V_e \end{bmatrix} = \mathbf{H}(s) \begin{bmatrix} V_h \\ F_e \end{bmatrix}, \mathbf{H}(s) = \begin{bmatrix} h_{11} & h_{12} \\ h_{21} & h_{22} \end{bmatrix} \tag{30}$$

where F_i and V_i, where $i \in [h, e]$ represents the operator and environment forces, and leader and follower velocities. We assume that the dynamics of the leader and follower are decoupled and predominantly linear or are controlled such that their apparent dynamics are observed as linear impedances. We further assume that the dynamics of the environment can be locally approximated by linear models, as such, the dynamics of the teleoperation system are

$$Z_{cm} V_h = F_h - F_{cm} \tag{31}$$
$$Z_{cs} V_e = F_{cs} - F_e \tag{32}$$

where $Z_{cm} := m_m s + b_m$ and $Z_{cs} := m_s s + b_s$ represent the leader and follower dynamics, F_{cm} and F_{cs} denote the control signals, V_h and V_e are the leader and follower velocities, F_h is the force exerted by the operator to the leader, and F_e is the force exerted by the environment to the follower. The control commands

$$F_{cm} = k_f F_e \tag{33}$$
$$F_{cs} = k_p (X_h - X_e) \tag{34}$$

implement a 2-channel P-F control architecture, where k_f and k_p are the force and position feedback gains, respectively, and X_h and X_e denote the leader and follower positions.

Using (31)–(34), the impedance matrix of the lumped LFN, denoted by the network N in Fig. 5, is given by

$$\begin{bmatrix} F_h \\ F_e \end{bmatrix} = \mathbf{Z} \begin{bmatrix} V_h \\ -V_e \end{bmatrix},$$
$$\mathbf{Z} = \begin{bmatrix} Z_{cm} + \frac{k_f k_p}{s} & k_f Z_{cs} + \frac{k_f k_p}{s} \\ \frac{k_p}{s} & Z_{cs} + \frac{k_p}{s} \end{bmatrix} \tag{35}$$

It is shown that the above LFN is A.S. iff the inequalities $m_s k_f k_p \le b_m b_s$ and $k_f k_p < (\sqrt{3}+2) b_m$ are satisfied [21].

Here, we will obtain the chain representation of network N. This representation facilitates breaking the network N into a distributed cascade of subnetworks N_1 and N_2. For information about chain representation, the reader is referred to the Appendix. Using the relation

$$\mathbf{T} = \frac{1}{Z_{21}} \begin{bmatrix} Z_{11} & \Delta \\ 1 & Z_{22} \end{bmatrix} \tag{36}$$

the corresponding chain matrix is obtained as

$$\begin{bmatrix} F_h \\ V_h \end{bmatrix} = \mathbf{T} \begin{bmatrix} F_e \\ V_e \end{bmatrix},$$
$$\mathbf{T} = \begin{bmatrix} \frac{sZ_{cm}}{k_p} + k_f & Z_{cm}(\frac{sZ_{cs}}{k_p} + 1) \\ \frac{s}{k_p} & \frac{sZ_{cs}}{k_p} + 1 \end{bmatrix} \tag{37}$$

It is easy to verify that cascading N_1 and N_2, as shown in Fig. 5, characterized by the chain matrices

$$\begin{bmatrix} F_h \\ V_h \end{bmatrix} = \mathbf{T}_1 \begin{bmatrix} E_2^{N_1} \\ F_2^{N_1} \end{bmatrix}, \ \mathbf{T}_1 = \begin{bmatrix} 1 & \frac{sZ_{cm}}{k_p} \\ 0 & \frac{s}{k_p} \end{bmatrix} \tag{38}$$

and

$$\begin{bmatrix} E_1^{N_2} \\ F_1^{N_2} \end{bmatrix} = \mathbf{T}_2 \begin{bmatrix} F_e \\ V_e \end{bmatrix}, \ \mathbf{T}_2 = \begin{bmatrix} k_f & 0 \\ 1 & (Z_{cs} + \frac{k_p}{s}) \end{bmatrix} \tag{39}$$

respectively, constitutes a distributed representation of the lumped network N. The scattering matrices needed for reflection coefficient calculation can be obtained from

$$\mathbf{S}_i = \left(\begin{bmatrix} 1 & -b \\ 0 & 0 \end{bmatrix} \mathbf{T}_i + \begin{bmatrix} 0 & 0 \\ 1 & b \end{bmatrix} \right)$$
$$\left(\begin{bmatrix} 1 & b \\ 0 & 0 \end{bmatrix} \mathbf{T}_i + \begin{bmatrix} 0 & 0 \\ 1 & -b \end{bmatrix} \right)^{-1} \tag{40}$$

As explained in the Appendix, the above split can implement a distributed control architecture as well, since the flow signal $F_2^{N_1}$ is a function of the leader network variable V_h and the effort signal $E_1^{N_2}$ is a function of the remote network variable F_e. Comparing (38) against the leader dynamics (31) shows that the leader subsystem reads control commands from the effort variable $E_2^{N_1}$, that is $F_{cm} = E_2^{N_1}$ and sends position feedback to the subsystem N_2 through $F_2^{N_1} = k_p X_h$. In the same manner, substituting $F_1^{N_2} = F_2^{N_1} = k_p X_h$ in $F_{cs} = F_1^{N_2} - k_p X_e$ implements the control signal $F_{cs} = k_p(X_h - X_e)$ in (34). The subnetwork N_2 also sends feedback through the effort variable $E_1^{N_2} = k_f F_e$ to the leader side to implement the control signal $F_{cm} = E_2^{N_1} = k_f F_e$ in (33).

Here, we will analyze the A.S. of the interconnection of N_1 and N_2 for the frequency range $0 \le \omega \le 200$ rad/s. The network parameters are set to

$$Z_{cm} = 0.1s + 2.5, \ Z_{cs} = 0.1s + 10,$$
$$k_f = 1, k_p = 20, b = 10. \tag{41}$$

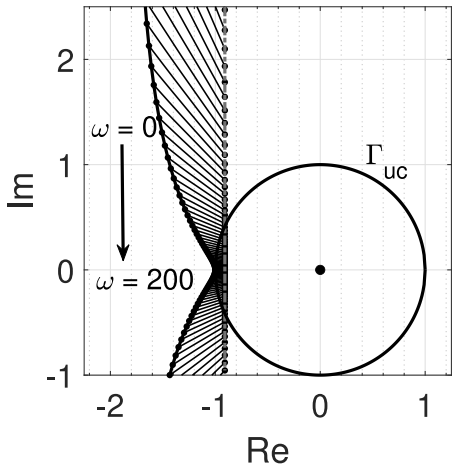

(a) $\Gamma_{in}^{N_2} = C(a_{N_2}, r_{N_2})$ for $\Gamma_2 = \Gamma_{uc}$; a_{N_2} is on the dotted line connected to $|a_{N_2}| + r_{N_2}$ through the inclined radii.

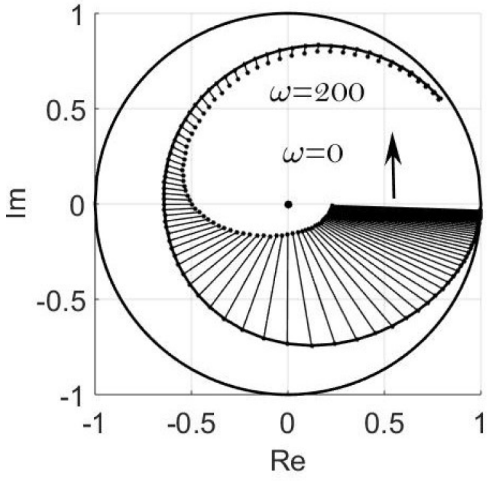

(b) $\Gamma_{in}^{N_1}$ for the load range denoted by $c(a_{N_2}, r_{N_2})$. Checking for $|\Gamma_{in}^{N_1}| < 1$ concludes the A.S. of the network N.

Fig. 6. A.S. analysis for the LFN in Fig. 5. Parameters are given by (41).

The Z_{cm} and Z_{cs} values represent the dynamics of the twin-pantograph haptic devices that will be used in the teleoperation experimental setup in Section 5.1. The analysis starts from finding the mapping of the unit circle $\Gamma_e = \Gamma_{uc}$ under the network N_2 for various frequencies, this is shown in Fig. 6(a). This results in a family of circles $C(a_{N_2}, r_{N_2})$ whose radii are represented by a set of line segments connecting the center a_{N_2} to the point on the circle with the largest distance from the origin, that is $|a_{N_2}| + r_{N_2}$. To obtain each circle associated with a frequency ω, the scattering matrix model for the network N_2 is used to obtain the scattering parameters for that frequency. These parameters in addition to $\Gamma_2 = \Gamma_{uc}$ are utilized in (18) to compute $\Gamma_{in}^{N_2}$ and then in (3) to derive the Möbius parameters ρ, θ, α and β. The Möbius parameters are then employed in (4) and (11) to obtain a_{N_2} and r_{N_2}.

The A.S. of the lumped network N can now be verified through analyzing bounded-Γ A.S. of N_1 for the load range $C(a_{N_2}, r_{N_2})$. The mapping of this load range through N_1 can be obtained using (24) and is shown in Fig. 6(b). Inclusion of $\Gamma_{in}^{N_1}$ within the unit circle concludes the A.S. of N. Convergence of the plot in Fig. 6(b) to a point inside the unit circle indicates that $\omega = 200$ rad/s is a large enough frequency upper-bound for numerical analysis.

As it can be seen in Fig. 6(a), the mapping $\Gamma_{in}^{N_2}$ does not lie within the unit disk. As a result, N_2 is potentially unstable. Also, it can be shown through Llewellyn's criteria that N_1 represented by

$$\begin{bmatrix} F_h \\ -F_2^{N_1} \end{bmatrix} = \begin{bmatrix} Z_{cm} & 1 \\ -\frac{k_p}{s} & 0 \end{bmatrix} \begin{bmatrix} V_h \\ E_2^{N_1} \end{bmatrix} \tag{42}$$

is not A.S. for any network N_1 parameter (i.e. M_m, b_m, K_p). Therefore, the coupled stability of N cannot be concluded through the traditional passivity approach, where at least one passive network with sufficiently large dissipative element is required to guarantee the passivity of cascade network N. For the absolute stability of N, this is not the case. While absolute stability of each cascade network is sufficient to guarantee the absolute stability of the network cascade, as seen from the potential instability of N_1 and N_2, the absolute stability of none of the networks is a necessary condition. This counts as an advantage of the proposed method, since each of the networks can be potentially unstable while the entire network is absolutely stable. In addition, the proposed chain-wise method provides a graphical representation of the circles for the range of frequency of interest and demonstrate how these circles migrate from one end of the network to the other end. This also provides an excellent opportunity to further investigate the effect of the leader and/or follower control parameters on the location and the size of the circles.

The graphical verification of bounded-Γ absolute stability, described earlier in Fig. 4, is plotted for the P-F control architecture in Fig. 7(a). The relative distance between stability region circles $C(a_{sr}, r_{sr})$ and load region circles $C(a_{lr}, r_{lr})$ is given by the distance between the points p_{lr} and p_{sr}. The dashed line and the corresponding circles are drawn for the maximum distance occurring at $\omega = 65$ rad/s. Fig. 7(b) denotes the distance for the frequency range $\omega = 0 \ldots 200$ rad/s. The larger the distance between p_{lr} and p_{sr} is, the larger the stability margin is for a given load range denoted by r_{lr}.

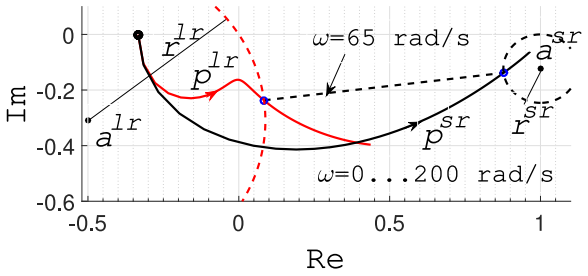

(a) The loci of points p^{lr} and p^{sr} for the range of frequencies $0 < \omega \leq 200$ rad/s are shown by solid lines.

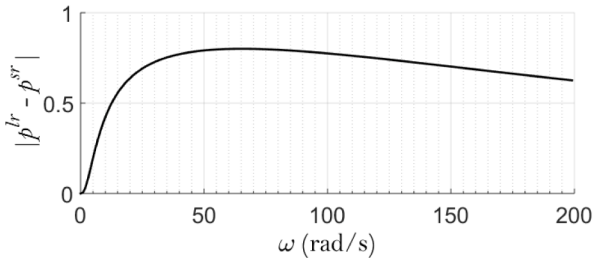

(b) The distance $|p^{lr} - p^{sr}|$ over the specified range of frequency.

Fig. 7. The relative distance between stability region circles $C(a_{sr}, r_{sr})$ and load region circles $C(a_{lr}, r_{lr})$ is a measure of stability robustness. The circles and the distance between the two circles for $\omega = 65$ rad/s are shown by dashed lines.

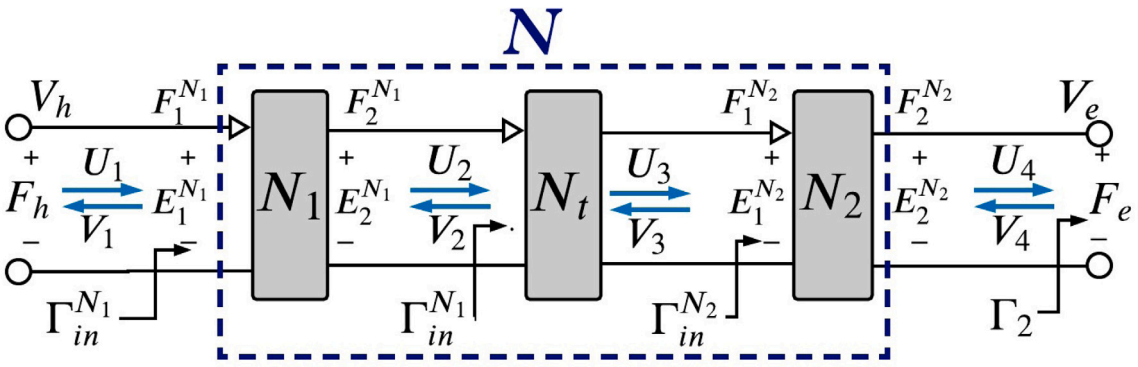

Fig. 8. Distributed representation of network N for the P-F architecture, with intervening tool impedance added.

4.2. Addition of a virtual coupling/tool

Virtual couplings or intervening impedances are introduced to enhance stability margin, add dynamics of a tool, or modify the range of perceived impedance by the operator [14,24,25].

One possible tool can be modeled by a parallel combination of mass and damper, or

$$\frac{1}{Z_t} = \frac{1}{m_t s} + \frac{1}{b_t}, \tag{43}$$

which can be interpreted as a damping term that increases in value as frequency increases [14]. Consider the P-F control architecture in Section 4.1. As shown in Fig. 8, the intervening impedance given by (43) is added between the leader and follower networks through the introduction of the tool network N_t characterized by

$$\begin{bmatrix} E_2^{N_1} \\ -F_1^{N_2} \end{bmatrix} = \mathbf{H}_t \begin{bmatrix} F_2^{N_1} \\ E_1^{N_2} \end{bmatrix}, \quad \mathbf{H}_t = \begin{bmatrix} sZ_t & 1 \\ -1 & 0 \end{bmatrix} \tag{44}$$

The added network N_t results in a change in the leader control signal $F_{cm} = k_f F_e + Z_t V_h$ in the P-F architecture.

The mapping of the passive load through the cascade $N_1 - N_t - N_2$ for the frequency range $\omega = 0 \dots 200$ rad/s, for the set of parameters given by (41) and the tool parameters

$$m_t = 0.1 \text{ kg}, \quad b_t = 0.6 \text{ Ns/m}, \tag{45}$$

are plotted in Fig. 9.

Since the added network N_t is between N_1 and N_2, the mapped unit circle under the network N_2 remains the same as the one plotted in Fig. 6(a), denoted by $\Gamma_{in}^{N_2} = C(a_{N_2}, r_{N_2})$. The network N_t maps $\Gamma_{in}^{N_2}$ to a more diverse region in the complex plane. The mapping $\Gamma_{in}^{N_t}$ under the network N_1 stays within the unit disk, as seen in Fig. 9(b), that is $\Gamma_{in}^{N_t}$ belongs to the stability region of N_1. As a result, the network N_1 is bounded-Γ A.S. for the load range $\Gamma_{in}^{N_t}$ and consequently the network N is A.S.

4.3. Delayed system in the power domain

We extend the network cascade for P-F control architecture to include a communication channel under constant time delay. A variable time delay can be rendered constant through buffering techniques such that the apparent delay in the channel is equal to the maximum upper bound on delays possible [38]. In this case, the delay network N_d is placed between the two sites, as shown in Fig. 10. Here, the power-domain signals $F_2^{N_1}$ and $E_2^{N_2}$ are transmitted between the leader and follower subnetworks.

The bounded-Γ A.S. analysis is performed for a round-trip time delay of 200 ms. The chain representation of the system include the three networks N_1, N_d, and N_2. The design starts from the case without time delay designed in Section 4.1, followed by the application of the

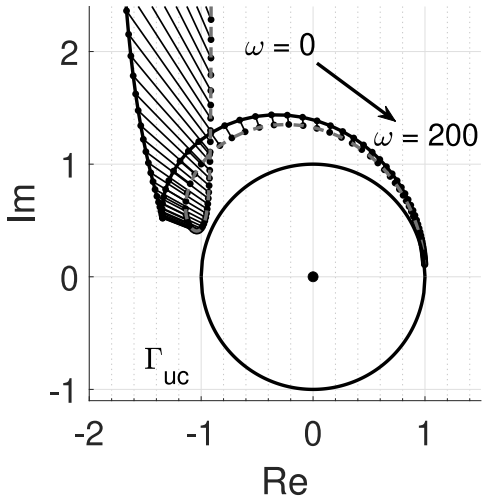

(a) The reflection coefficient $\Gamma_{in}^{N_t}$ resulted from the mapping $\Gamma_{in}^{N_2}$ under the network N_t. Note that $\Gamma_{in}^{N_2}$ is already depicted in Fig. 6.

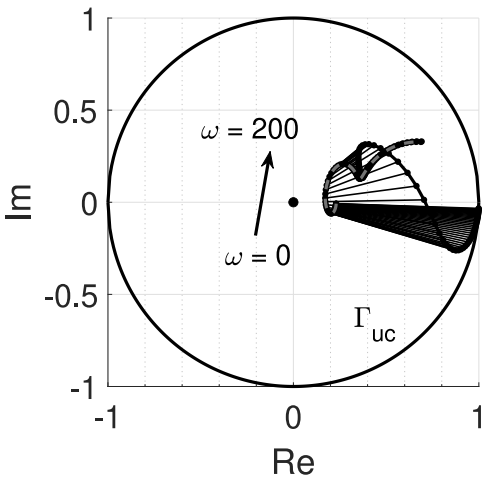

(b) Bounded-Γ A.S. of N_1.

Fig. 9. A.S. analysis for the LFN with virtual tool. Parameters are given by (41) and (45).

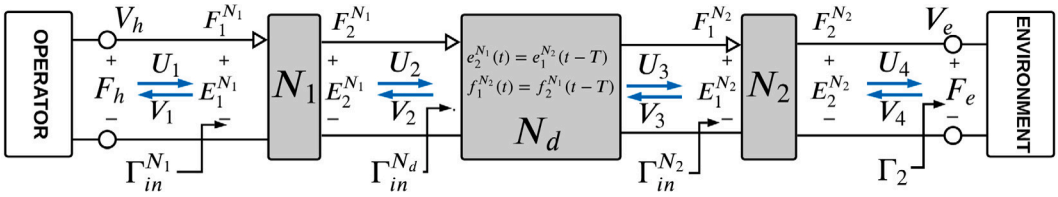

Fig. 10. Chain representation of the P-F architecture under constant delay between two sites. Consecutive evaluation of input reflection coefficient of each network can be conducted to obtain the range of $\Gamma_{in}^{N_1}$.

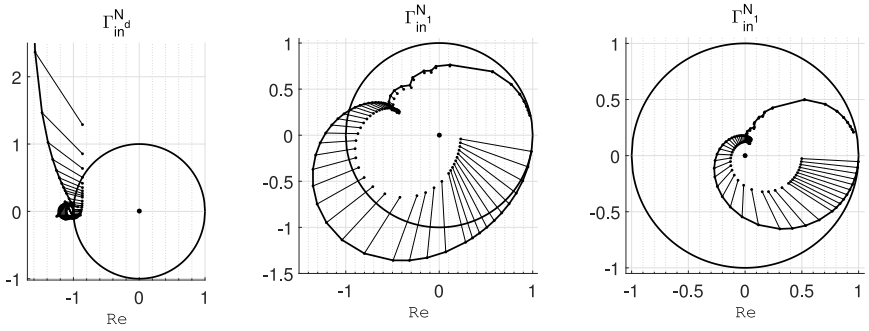

(a) Potentially unstable system (b) Stabilizing the system

Fig. 11. Development of an A.S. lumped network through analyzing bounded-Γ A.S. of N_1. (a) T=100 ms, $b_m = 3$, $b_s = 10$ Ns/m, $k_f = 1$, $k_p = 30$ (b) Increasing the damping gain to $b_m = 10$ Ns/m confines $\Gamma_{in}^{N_1}$ to unit disk.

chain analysis method to update the network parameters in the cascade such that the lumped LFN is A.S.

As explained in Section 3.3, we start from the last network in the cascade where the load is denoted by passivity unit circles and continue tracking the loci of the circles until we find the location of the mapped circles at the operator side, that is $\Gamma_{in}^{N_1}$. The input reflection coefficient $\Gamma_{in}^{N_2}$ is already calculated and plotted in Fig. 6(a) for $\Gamma_2 = \Gamma_{uc}$. The resulting circles are denoted by $C(a_{N_2}, r_{N_2})$. These circles are used as the termination load for network N_d to calculate the input reflection coefficient $\Gamma_{in}^{N_d}$ from (18) using the scattering parameters for the network N_d, that is

$$\mathbf{S}_d = \begin{bmatrix} -\tanh(jT\omega) & 1/\cosh(jT\omega) \\ 1/\cosh(jT\omega) & \tanh(jT\omega) \end{bmatrix}. \tag{46}$$

The chain analysis for the set of parameters from Section 4.1 shows that the lumped LFN is not A.S. under time delay [see Fig. 11(a)]. Calculating input reflection coefficient $\Gamma_{in}^{N_d}$ for the set of circles $C(a_{N_2}, r_{N_2})$ gives the new set of circles $C(a_{N_d}, r_{N_d})$.

We make the LFN A.S. by enclosing the input reflection coefficient $\Gamma_{in}^{N_1}$ within the unit disk, as shown in Fig. 11(b). This is achieved by increasing the leader damping gain to $b = 10Ns/m$, thereby confining $\Gamma_{in}^{N_d}$ to the unit disk. It was mentioned earlier that increasing damping in an impedance leads to smaller circle mapping of its corresponding reflection coefficient [15]. Other approach would be to introduce a low-pass filter in the communication channel. This approach works well for cases where wave variables are transmitted, because low-pass filter in the scattering-domain is a passive transfer function.

It is noteworthy that the proposed approach aims at achieving A.S. for LFN and not passivity. As a result, none of the cascade subnetworks needs to be passive. In fact, in our case, N_1, N_2, and N_d are all active, yet the network N is A.S. The goal of achieving an A.S. LFN allows us to transmit explicit position signals, which remedies the position drift problem associated with the transmission of wave variables [16,26].

5. Experimental results and discussion

Although it is challenging to experimentally investigate A.S. of an LFN by trying with all possible terminations as seen in [23], it is possible to demonstrate potential instability with a specific passive environment. We investigate the coupled stability of our teleoperator with the P-F controller under the three conditions studied in Figs. 10 and 11.

5.1. Experimental setup & procedure

In this section, the absolute stability of the position–force bilateral control architecture in (32)–(34) is experimentally implemented on an experimental test-bed. The experimental setup consists of two Quanser planar twin-Pantograph haptic devices used as the leader and the follower, see Fig. 12. Each Pantograph is actuated by four direct-drive DC motors and provides three degrees of freedom at its end-point, two translational and one rotational. The angle of rotation of each motor is measured by a high-resolution encoder with 20,000 counts/rev. Each Pantograph is equipped with an ATI Nano-25 force/torque sensor that allows for the measurement of operator and environment forces. The control systems are implemented at the sampling rate of 1 KHz. In our experiments, we restricted the motion to the Y direction. The same control parameters used in Section 4.3 are utilized for the cases of $T = 0$ and 100 ms. The procedure for the experiments is as follows: The human operator displaced the leader haptic device along its y-axis, while the follower device follows the trajectory of the leader until it comes in contact with a rigid environment at ≈ 44 mm. The operator attempts to command the follower to move further into the environment for a few seconds, before withdrawing. The action is repeated.

5.2. Experimental results

Fig. 13 demonstrates the leader and the follower forces and positions for time delays $T = 0$ ms and $T = 100$ ms. As seen from Fig. 13(a) and expected from the analysis in Section 4.3, the coupled system should remain stable for $T = 0$ ms and $b_m = 3$ Ns/m, as the LFN is A.S. The controller is a two-channel P-F architecture; as such it does not provide perfect transparency when delay is negligible. This can be seen from the errors in the position and force tracking plots. As shown in Fig. 13(b), the same system once the delay increases to

Fig. 12. Experimental setup consisting of two twin-Pantographs.

$T = 100$ ms becomes unstable. This corresponds with the potentially unstable results that our Möbius analysis converged to in Section 4.3. Increasing the damping gain b_m to 10 Ns/m in Fig. 13(c) makes the LFN A.S. and stabilizes the coupled system in the presence of the time delay. This comes at a cost to the performance of the system in free motion, as the amount of force the operator needs to exert to move the leader has risen substantially.

5.3. Discussion

The case study showcased the modularity of the proposed method in analyzing coupled stability of cascaded systems. The experiments also demonstrated the potential instability of the network as determined by theory. Below, we will provide an overview of the process of applying the proposed method and a discussion on some of the practical aspects and limitations of the method.

For a given teleoperation system, if the teleoperator dynamics including the dynamics of the leader and follower and the intermediate dynamics (e.g. delays, virtual coupling, ...) can be linearized about an operating point or linearized through control (e.g. inverse dynamics, feedback linearization,...), the proposed methodology can be applied. For the cases where the nonlinearity is significant and cannot be mitigated, the proposed methodology cannot be applied as presented. If the dynamics of any of the two-port networks depend on more than two parameters, and we wish to investigate the effect of each parameter on A.S., we can break the two-port network using chain representation technique discussed in Section 4.1 and Appendix. We then start from the last network in the cascade where its load (environment) is denoted by the passivity unit circle in the scattering domain. We apply the Möbius transformation (18) to track the loci of the circles for a range of frequencies of interest from one subnetwork, to the next until we find the location of the mapped circles at the operator side, that is $\Gamma_{in}^{N_1}$. If these circles are contained in the unit circle, then the network N is A.S.; otherwise, the network is potentially unstable. In that case, the absolute stability of the network would then be guaranteed through ensuring the bounded-Γ absolute stability of the last network in the chain by making sure that the load for the subnetwork N_1 is in the stability region of N_1, or the condition (28) is satisfied, where a_{sr} and r_{sr} can be found by applying the unit circle $\Gamma_{in} = \Gamma_{uc}$ to (26).

In the proposed method, the circles are tracked using the subnetwork models. In the case of inaccurate modeling or dynamic disturbances, the location and size of the circles will change. Therefore, in such cases, some measures of robustness can be added by making the region that Γ^{N1} covers over frequencies of interest contained in a circle with a radius smaller than unity. This way for sufficiently small inaccuracies or dynamic disturbances, the mapped circles will not grow out of the unit circle. In addition, an experimental (data-driven) method has been proposed in [23] to assess a network A.S. In this method, the circles resulting from all passive loads can be constructed by applying three distinct experiments, namely free motion, clamped and mass carrying follower. Such methods can be applied to the last subnetwork, namely N_r.

One of the benefits of our proposed method as demonstrated in the case study is that it can be used for passive or active subnetworks. It should be noted that Llewellyn's criterion has also been used with active terminations [39]. However, the criterion is only applicable to a class of active terminations that can be presented as all passive dynamics in series and/or parallel combination with active components. These active components in then absorbed into the LFN and the Llewellyn's is applied to the modified LFN. The proposed method in the paper does not have limitation on the nature of the active components and has a broader application.

6. Conclusions

In this article, the geometric interpretation of Möbius transformation has been utilized for the analysis of coupled stability of leader–follower networks. Based on the symmetry principle of Möbius transformation, a new proof of absolute stability condition in scattering domain for two-port networks is provided.

A distributed representation of a lumped leader–follower network was presented through an example of a force-position control architecture. A chain-wise analysis of coupled stability of the cascade was proposed which progressively derives the mapping of all passive loads through the cascade to the leader side. Then, the absolute stability of the entire network would then be guaranteed through ensuring the bounded-Γ absolute stability of the last network in the chain. The advantage of the proposed method was demonstrated through coupled stability analysis of the position–force control architecture under constant time delay. Numerical analysis shows that passivity methods cannot be used as the communication channel would not be passive when explicit position feedback is transmitted.

A criterion for absolute stability of multi-DOF teleoperation systems has been presented in [19], however, possible future work will focus on extending the proposed method to multi-DoF teleoperation systems. Also worth exploring is if an architectural challenge arises in multi-user systems where two leaders collaborate with one follower in a shared environment.

CRediT authorship contribution statement

Kamran Razi: Conceptualization, Methodology. **Chiedu N. Mokogwu:** Data curation, Writing – orginal draft, Visualization, Investigation. **Keyvan Hashtrudi-Zaad:** Supervision, Validation, Writing.

Declaration of competing interest

The authors declare that they have no known competing financial interests or personal relationships that could have appeared to influence the work reported in this paper.

Acknowledgments

This work was supported in part by Natural Sciences and Engineering Research Council of Canada (NSERC).

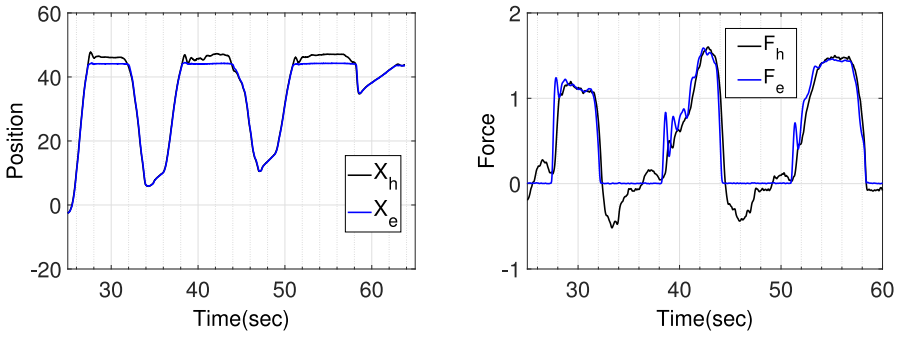

(a) T=0 ms, b_m=3

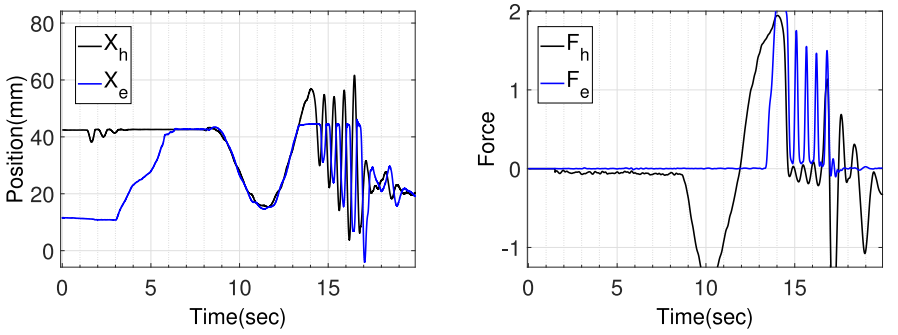

(b) T=100 ms, b_m=3

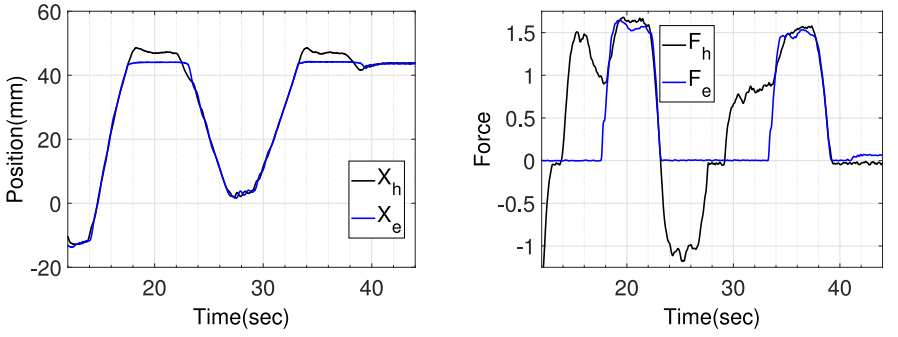

(c) T=100 ms, b_m=10

Fig. 13. Experimental results for the P-F control architecture under constant time delay discussed in Section 4.3.

Appendix. Chain representation of networks

Consider the chain representation of the network N in Fig. 5 given by

$$\begin{bmatrix} E_1^{N_1} \\ F_1^{N_1} \end{bmatrix} = \begin{bmatrix} T_{11} & T_{12} \\ T_{21} & T_{22} \end{bmatrix} \begin{bmatrix} E_2^{N_2} \\ F_2^{N_2} \end{bmatrix} = \mathbf{T} \begin{bmatrix} E_2^{N_2} \\ F_2^{N_2} \end{bmatrix} \tag{A.1}$$

where $\mathbf{T}$ denotes the chain matrix of the network N. Chain representation facilitates stability and performance analysis as well as controller design for network cascades. The reason being is that if a network is a cascade of multiple subnetworks, the chain representation of the entire network is found by post multiplication of the matrices associated with each subnetwork. For instance, if N is obtained by cascading the subnetworks N_1 and N_2, then

$$\mathbf{T} = \mathbf{T}_1\mathbf{T}_2 \tag{A.2}$$

where $\mathbf{T}_i$ is the chain representation of the network N_i, i=1,2. In a teleoperation setup with the leader and the follower at different locations, the representation (A.2) provides a distributed control architecture if $\mathbf{T}_1$ and $\mathbf{T}_2$ are each a function of one site parameters. This requirement is placed to guarantee that the transmitted feedback information at the leader site, for example, is not a function of remote site sensory information.

It is noteworthy that the distributed representation is not unique. For example, if a representation is associated with the chain matrix decomposition $\mathbf{T} = \mathbf{T}_1\mathbf{T}_2$, the following decomposition also gives other representations

$$\mathbf{T} = (\mathbf{T}_1\mathbf{T}_c)(\mathbf{T}_c^{-1}\mathbf{T}_2), \tag{A.3}$$

for an invertible matrix $\mathbf{T}_c$.

References

[1] Schmaus P, Leidner D, Krüger T, Bayer R, Pleintinger B, Schiele A, et al. Knowledge driven orbit-to-ground teleoperation of a robot coworker. IEEE Robot Autom Lett 2019;5(1):143–50.

[2] Shukla A, Karki H. Application of robotics in offshore oil and gas industry-a review part ii. Robot Auton Syst 2016;75:508–24.
[3] Panzirsch M, Balachandran R, Weber B, Ferre M, Artigas J. Haptic augmentation for teleoperation through virtual grasping points. IEEE Trans Haptics 2018;11(3):400–16.
[4] Mohand-Ousaid A, Haliyo S, Régnier S, Hayward V. High fidelity force feedback facilitates manual injection in biological samples. IEEE Robot Autom Lett 2020;5(2):1758–63.
[5] Seifabadi R, Rezaei SM, Ghidary SS, Zareinejad M. A teleoperation system for micro positioning with haptic feedback. Int J Control Autom Syst 2013;11(4):768–75.
[6] Atashzar SF, Shahbazi M, Tavakoli M, Patel RV. A passivity-based approach for stable patient-robot interaction in haptics-enabled rehabilitation systems: modulated time-domain passivity control. IEEE Trans Control Syst Technol 2016;25(3):991–1006.
[7] Shahbazi M, Atashzar SF, Ward C, Talebi HA, Patel RV. Multimodal sensorimotor integration for expert-in-the-loop telerobotic surgical training. IEEE Trans Robot 2018;34(6):1549–64.
[8] Frishman S, Kight A, Pirozzi I, Coffey MC, Daniel BL, Cutkosky MR. Enabling in-bore mri-guided biopsies with force feedback. IEEE Trans Haptics 2020;13(1):159–66.
[9] Hogan N. Controlling impedance at the man/machine interface. In: Proc. IEEE international conference on robotics and automation. 1989, p. 1626–7.
[10] van der Schaft A. L2-gain and passivity techniques in nonlinear control. Springer Verlag; 2000.
[11] Ousaid AM, Haliyo DS, Régnieregnier S, Hayward V. A stable and transparent microscale force feedback teleoperation system. IEEE/ASME Trans Mechatronics 2015;20(5):2593–603.
[12] Haykin S. Active network theory. Addison-Wesley Pub. Co. 1970.
[13] Llewellyn F. Some fundamental properties of transmission systems. Proc IRE 1952;40(3):271–83.
[14] Adams RJ, Hannaford B. Stable haptic interaction with virtual environments. IEEE Trans Robot Autom 1999;15(3):465–74.
[15] Haddadi A, Hashtrudi-Zaad K. Bounded-impedance absolute stability of bilateral teleoperation control systems. IEEE Trans Haptics 2010;15–27.
[16] Haddadi A, Hashtrudi-Zaad K. Robust stability of teleoperation systems with time delay: A new approach. IEEE Trans Haptics 2013;6(2):229–41.
[17] Haddadi A, Razi K, Hashtrudi-Zaad K. Operator dynamics consideration for less conservative coupled stability condition in bilateral teleoperation. IEEE/ASME Trans Mechatronics 2015;20(5):2463–75.
[18] Khademian B, Hashtrudi-Zaad K. Dual-user teleoperation systems: New multilateral shared control architecture and kinesthetic performance measures. IEEE/ASME Trans Mechatronics 2011;17(5):895–906.
[19] Li J, Tavakoli M, Huang Q. Absolute stability of multi-dof multilateral haptic systems. IEEE Trans Control Syst Technol 2014;22(6):2319–28.
[20] Tugal H, Carrasco J, Falcon P, Barreiro A. Stability analysis of bilateral teleoperation with bounded and monotone environments via zames–falb multipliers. IEEE Trans Control Syst Technol 2016;25(4):1331–44.
[21] Razi K, Hashtrudi-Zaad K. Analysis of coupled stability in multilateral dual-user teleoperation systems. IEEE Trans Robot 2014;30(3):631–41.
[22] Razi K, Hashtrudi-Zaad K. Development of a guaranteed stable network of telerobots with kinesthetic consensus. IEEE Trans Haptics 2014;7(4):454–66.
[23] Mokogwu CN, Razi K, Hashtrudi-Zaad K. Experimental assessment of absolute stability in bilateral teleoperation. IEEE Trans Haptics 2020;13(3):380–92.
[24] Sirouspour S. Modeling and control of cooperative teleoperation systems. IEEE Trans Robot 2005;21(6):1220–5.
[25] Yokokohji Y, Yoshikawa T. Bilateral control of master–slave manipulators for ideal kinesthetic coupling-formulation and experiment. IEEE Trans Robot Autom 1994;10(5):605–20.
[26] Niemeyer G, Slotine J-J. Stable adaptive teleoperation. IEEE J Ocean Eng 1991;16(1):152–62.
[27] Chen Z, Huang F, Chen W, Zhang J, Sun W, Chen J, et al. RBFNN-based adaptive sliding mode control design for delayed nonlinear multilateral telerobotic system with cooperative manipulation. IEEE Trans Ind Inf 2019;16(2):1236–47.
[28] Chen Z, Huang F, Sun W, Gu J, Yao B. RBF-neural-network-based adaptive robust control for nonlinear bilateral teleoperation manipulators with uncertainty and time delay. IEEE/ASME Trans Mechatronics 25(2):906–18.
[29] Bacocco R, Borghesan G, Melchiorri C. Experimental evaluation of two control schemes for cooperative teleoperation. In: Proc. IEEE world automation congress 2012. 2012, p. 1–6.
[30] Agarwal E, Sivaranjani S, Gupta V, Antsaklis P. Compositional verification of passivity for cascade interconnected nonlinear systems. In: Proc. IEEE 28th mediterranean conference on control and automation. 2020, p. 319–24.
[31] Mokogwu C, Hashtrudi-Zaad K. Energy-based analysis of string stability in vehicle platoons. IEEE Trans Veh Tech http://dx.doi.org/10.1109/TVT.2022.3158624.
[32] Razi K, Hashtrudi-Zaad K. Möbius transformation and application to coupled stability analysis of cascaded master and slave networks. In: Proc. IEEE haptics symposium. 2014, p. 539–44.
[33] Needham T. Visual complex analysis. Oxford University Press; 1998.
[34] Hahn L. Complex numbers and geometry. In: MAA spectrum. Vol. 495. second ed.. Cambridge University Press; 1996.
[35] Hashtrudi-Zaad K, Salcudean S. Analysis of control architectures for teleoperation systems with impedance/admittance master and slave manipulators. Int J Robot Res 2001;20(6):419–45.
[36] Mokogwu CN, Hashtrudi-Zaad K. A hybrid position–rate teleoperation system. Robot Auton Syst 2021;141:103781.
[37] Edwards ML, Sinsky JH. A new criterion for linear two-port stability using a single geometrically derived parameter. IEEE Trans Microw Theory Tech 1992;40(12):2303–11.
[38] Kosuge K, Murayama H, Takeo K. Bilateral feedback control of telemanipulators via computer network. In: Proc. IEEE/RSJ international conference on intelligent robots and systems. Vol. 3. 1996, p. 1380–5.
[39] Li W, Ding L, Gao H, Tavakoli M. Haptic tele-driving of wheeled mobile robots under nonideal wheel rolling, kinematic control and communication time delay. IEEE Trans Syst Man Cybern Syst 2020;50(1):336–47.

Kamran Razi (M07) received his Ph.D. degree from Queen's University, Kingston, Canada, in 2014 and his M.Sc. degree from Center of Excellence for Control and Intelligent Processing (CIPCE), University of Tehran in 2007, both in Electrical Engineering. He is currently with Fortinet Inc., Burnaby, Canada, where his work focuses on application of machine learning algorithms and AI to enhance cybersecurity. Dr. Razi's research interest lies in haptics, real-time control systems, embedded system design and machine learning.

Chiedu N. Mokogwu (M10) received his B.Sc. degree in Computer Engineering from the University of Benin in 2006, and M.Sc. degree from University of Sheffield in Control Systems, 2010. He received his doctorate degree from the Department of Electrical and Computer Engineering, Queen's University, Kingston, Ontario, Canada in 2021. He is currently a Research Associate at the BioRobotics Research Lab in the Department of Electrical and Computer Engineering, Queen's University, Kingston, Ontario. Chiedu Mokogwu is a member of the IEEE and his current research interests include control systems design and analysis for of leader–follower multi-agent, haptic, telerobotic systems and application of artificial intelligence/machine learning for autonomous driving.

Keyvan Hashtrudi-Zaad (SM08) received his Ph.D. degree in Electrical and Computer Engineering from the University of British Columbia, Vancouver, Canada, in 2000. He then held a consulting position with Motion Metrics International Corporation, Vancouver, where he worked on the development of a dynamic payload monitoring system for heavy duty hydraulic machines. In 2001, he joined the Department of Electrical and Computer Engineering, Queen's University, Kingston, Ontario, Canada, where he is currently a Professor and the Director of BioRobotics Research Laboratory. Dr. Hashtrudi-Zaad's research interests include haptics, telerobotics, mechatronics, and controls and their applications in telerehabilitation, medical interventions and self-driving vehicles. Dr. Hashtrudi-Zaad is an Associate Editor of IEEE Robotics and Automation Letters and the General Co-Chair of the IEEE World Haptics Conference 2021. He has also served as an Associate Editor of the IEEE Transactions on Haptics and a co-organizer of several IEEE sponsored conferences.